Journal of Solid State Chemistry 183 (2010) 46–51

Contents lists available at ScienceDirect

Journal of Solid State Chemistry

journal homepage: www.elsevier.com/locate/jssc

Ab-initio study of the structural, linear and nonlinear optical properties of $CdAl_2Se_4$ defect-chalcopyrite

T. Ouahrani [a], Ali H. Reshak [b,*], R. Khenata [c], B. Amrani [c], M. Mebrouki [a], A. Otero-de-la-Roza [d], V. Luaña [d]

[a] Laboratoire de Physique Théorique, B.P. 119, Université de Tlemcen, Tlemcen 13000, Algeria
[b] Institute of Physical Biology, South Bohemia University, Nove Hrady 37333, Czech Republic
[c] Laboratoire de Physique Quantique et de Modélisation Mathématique, (LPQ3M), Université de Mascara, Mascara 29000, Algeria
[d] Departamento de Química Física y Analítica, Universidad de Oviedo, 33006 Oviedo, Spain

ARTICLE INFO

Article history:
Received 14 July 2009
Received in revised form
11 September 2009
Accepted 27 September 2009
Available online 22 October 2009

PACS:
70
71.15.Ap
71.15.–m

Keywords:
FP-LAPW
GGA-WC
Electronic properties
Linear and nonlinear optical properties

ABSTRACT

The complex density functional theory (DFT) calculations of structural, electronic, linear and nonlinear optical properties for the defect chalcopyrite $CdAl_2Se_4$ compound have been reported using the full potential linearized augmented plane wave (FP-LAPW) method as implemented in the WIEN2k code. We employed the Wu and Cohen generalized gradient approximation (GGA-WC), which is based on exchange–correlation energy optimization to calculate the total energy. Also we have used the Engel–Vosko GGA formalism, which optimizes the corresponding potential for band structure, density of states and the spectral features of the linear and nonlinear optical properties. This compound has a wide direct energy band gap of about 2.927 eV with both the valence band maximum and conduction band minimum located at the center of the Brillouin zone. The ground state quantities such as lattice parameters (a, c, x, y and z), bulk modulus B and its pressure derivative B' are evaluated. We have calculated the frequency-dependent complex $\varepsilon(\omega)$, its zero-frequency limit $\varepsilon_1(0)$, refractive index $n(\omega)$, birefringence $\Delta n(\omega)$, the reflectivity $R(\omega)$ and electron energy loss function $L(\omega)$. Calculations are reported for the frequency-dependent complex second-order nonlinear optical susceptibilities. We find opposite signs of the contributions of the 2ω and 1ω inter/intra-band to the imaginary part for the dominant component through the wide optical frequency range.

1. Introduction

Most of ternary adamantine semiconductors with the chemical formula $A^{II}B_2^{III}C_4^{IV}$ crystallize in the defect chalcopyrite (DC) tetragonal structure. This structure is close to the chalcopyrite (CH) [1], expect that the DC compounds contain a crystallographically ordered array of vacancies (stoichiometric voids or vacancies) in the cation sub-lattice. The low packing efficiency of constituent atoms in lattice facilitates the doping of DC compounds by impurities and the formation of solid solutions. Defect chalcopyrite ordered vacancy compounds are a class of materials with high technological interest due to their semiconducting properties, broad band gaps, and potential applications in linear, nonlinear optical and photovoltaic devices [2–5]. In particular, tunable filters based on $CdGa_2S_4$ and UV photo-detectors based on $CdAl_2Se_4$ are already used as devices [6,7]. The $A^{II}B_2^{III}C_4^{IV}$ compounds concerned in this paper have cadmium as the group II element, aluminum as the group III element, and selenium as the group IV element. $CdAl_2Se_4$ is an interesting ordered-vacancy compound, of which many experimental studies exist [3–5,8,12]. The $CdAl_2Se_4$ single crystal was grown by the chemical vapor transport method [5]. Spectroscopic ellipsometry and polarized transmission intensity measurements have been used to characterize the optical properties of the ordered-vacancy of this later [4]. X-ray diffraction study at 80 K and at high pressure is also reported by Meenakshi and coworkers [9], they observe a transformation of the (DC) $CdAl_2Se_4$ to a disordered rock salt type structure and after decompression into a disordered zinc-blende type structure. Range et al. [10] observed a phase change to spinel structure at 4.5 GPa and 400 °C. From the theoretical viewpoint, Jiang and Lambrecht [11] have investigated the band structure and band gaps of defect chalcopyrite compounds using the linear muffin-tin orbital (LMTO) method.

Recently, several experimental studies have been performed to determine its optical and vibrational properties at zero pressure [3,4,12]. To our knowledge a theoretical study of the electronic and optical properties of the investigated compound has not yet been undertaken. Therefore, we think that it is timely to perform first-principles calculations for structural and optoelectronic calculations within full potential linearized augmented plane wave

* Corresponding author. Fax: +420 386 361231.
E-mail address: maalidph@yahoo.co.uk (A.H. Reshak).

0022-4596/$ - see front matter © 2009 Elsevier Inc. All rights reserved.
doi:10.1016/j.jssc.2009.09.034

(FP-LAPW) method [13,14]. Hence the effect of the full potential on the linear and nonlinear optical properties can be ascertained.

The rest of the paper has been divided in three parts. In Section 2, we briefly describe the computational techniques used in this study. The most relevant results obtained for the structural, electronic and optical properties of $CdAl_2Se_4$ compound are presented and discussed in Section 3. Finally we summarize the main conclusions of our work in Section 4.

2. Computational details

Self-consistent FP-LAPW [13,14] calculations on $CdAl_2Se_4$ were carried out using WIEN2k package [15]. An adequate trade-off between accuracy and cost was achieved by considering a number of basic functions up to $R_{MT} \times K_{max}=9$, where R_{MT} is the minimum radius of the muffin-tin spheres and K_{max} gives the magnitude of the largest K vector in the plane wave basis. In order to keep the same degree of convergence, we kept the values of the sphere radii and K_{max} constant over all the crystal geometries considered. We have chosen the muffin-tin radii R_{MT} for Cd, Al and Se to be 2.44, 2.11 and 2.2 atomic units (a.u), respectively. Additionally, the valence wave functions inside muffin-tin spheres are expanded up to $l_{max}=10$. The exchange and correlation effects are treated by the Wu and Cohen generalized gradient approximation (GGA-WC) functional [16]. Apart from the standard local density approximation (LDA) and GGA (PBE), a more accurate [17] nonempirical density functional generalized gradient approximation (GGA), as proposed by Wu and Cohen for the exchange–correlation energy, E_{xc}, has been attempted in these calculations. The dependence of the energy on the number of k points in the irreducible wedge of the Brillouin zone (IBZ) has been checked, and the size of the mesh has been set to $10 \times 10 \times 10$ points. Self-consistency is considered to be reached when the total energy difference between successive iterations is $< 10^{-5}$ Ry per formula unit.

The crystal arrangement of our DC is formally similar to the chalcopyrite structure. The A and B cations still form separate AC_4 and BC_4 tetrahedra, but the anion is now surrounded by one B atom, one A atom and one vacant site, whereas the tetragonal unit-cell of the DC compound is formed by roughly doubling the zinc-blende unit cell along a preferred (c-) direction; the ordering may result in a tetragonal distortion defined by $\eta = c/2a < 1$; c and a being the lattice parameters. The basic lattice vectors can be chosen as $2A(0,0,0)$, $2B^1(0,0,0.5)$, $2B^2(0,0.5,0.25)$ and $8C(x, y, z)$, where (x, y, z) are the internal positions parameter for the C atom.

3. Results and discussion

3.1. Structural properties

The internal structure parameters, x, y and z, describing the position of Se atom and the (c/a) ratio are optimized. The obtained values are used to investigate the structural properties. By calculating the total energy at different volumes and fitting the resulting $E(V)$ curve to the empirical Murnaghan equation of state [18], the equilibrium volume, lattice constants, bulk modulus B and its first pressure derivative B' were obtained. Table 1 displays the values of the obtained structural properties compared to previous experimental and theoretical results. Our calculated structural properties show good agreement with the available experimental results [5,8] and the previous theoretical calculation using PBE96-GGA and LDA [3]. We notice that our bulk modulus B and its first-order pressure derivative B' are overestimated compared with PBE96-GGA and LDA results. We would like to mention that there is no experimental data for the bulk moduli of this compound in the literature.

Table 1
The lattice constant a, the c/a ratio and the internal parameters (x, y, z), the bulk modulus B and its first derivative B' of $CdAl_2Se_4$ compared to experimental and theoretical values.

	This work	Experimental	Theoretical
a (Å)	5.7474	5.7606[a] 5.740[b]	5.67[c] 5.86[d]
c/a	1.8713	1.86[a] 1.84[b]	1.86[c] 1.86[d]
x	0.2742	0.2686[a] 0.272[b]	0.276[c] 0.270[d]
y	0.2620	0.267[a] 0.261[b]	0.259[c] 0.269[d]
z	0.1388	0.1366[a] 0.138[b]	0.140[c] 0.137[d]
B	59.854	–	40.1[c] 31.479[d]
B'	4.2444	–	5.395[c] 5.143[d]

[a] Ref. [6].
[b] Ref. [9].
[c] LDA Ref. [3].
[d] GGA91 Ref. [3].

3.2. Optoelectronic properties

It is well known in the self-consistent band structure calculation within DFT, both LDA and GGA usually underestimate the energy gap [19]. This is mainly due to the fact that they are based on simple model assumptions which are not sufficiently flexible to accurately reproduce the exchange correlation energy and its charge derivative. Engel and Vosko considered this shortcoming and constructed a new functional form of GGA [20] which is able to better reproduce the exchange potential at the expense of less agreement in the exchange energy. This approach called EV-GGA, yields better band splitting and some other properties which mainly depend on the accuracy of exchange correlation potential. The Engel–Vosko GGA approximation [20] seems to yield better band splitting compared to LDA and GGA. Therefore, it is useful to use the EV-GGA for the electronic and optical properties [21,22].

3.2.1. Band structure and density of states

The calculated electronic band structures along the symmetry points of the Brillouin zone and the total densities of states (DOS) of the $CdAl_2Se_4$ compound are shown in Fig. 1. The overall profile of the valence and conduction bands configuration of our calculated band structures is in fairly good agreement with previous theoretical calculations [3,11]. The valence band maximum (VBM) and the conduction band minimum (CBM) are located at the Γ point resulting in a direct band gap of about 2.927 eV. Our calculated energy band gap is very close to the experimental one (3.07 eV) obtained by Krauß et al. [5].

The valence band region of the band structure is about 13.0 eV wide, and it is divided into three sets we will call them as low-, intermediate-, and higher-energy sets of bands. We have analyzed the contribution of the anion and cations states to each set of bands by decomposing the DOS into s-, p-, and d-orbital contributions. The result is the site-projected partial density of states shown in Fig. 2a–c. The low-energy set of valence bands (-12.72 to -11.24 eV) are derived from Se-s orbitals with a small contribution from Cd-d orbitals (-7.75 to -7.40 eV). The intermediate-energy set of valence bands are derived from the semi-core Cd-d orbitals. The higher-energy set of valence bands can be further divided into two sub-bands. The lower-energy sub-band from -5.5 to -3.2 eV is an Al-s and Se-p bands. The higher-energy sub-band from -3.2 eV up to Fermi energy (E_F) is a Se-p band with a small contribution from Al-p, Cd-d and Cd-s orbitals.

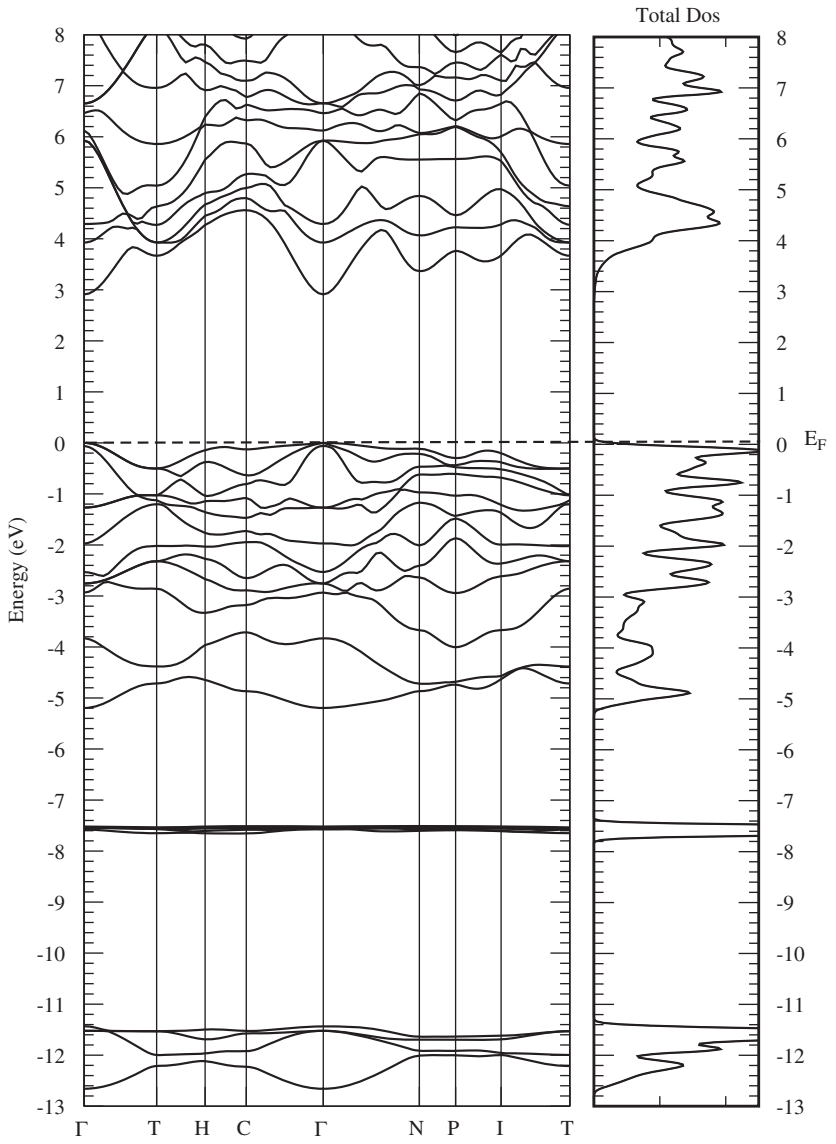

Fig. 1. Calculated band structure and total density of $CdAl_2Se_4$.

3.2.2. Linear optical properties

The investigated compound crystallizes in the $I\bar{4}$ space group. This symmetry group has two dominant components of the dielectric tensor. These dielectric functions are $\varepsilon_2^{\perp}(\omega)$ and $\varepsilon_2^{\parallel}(\omega)$, corresponding to the electric field direction parallel and perpendicular to the crystallographic *c* axis. The calculation of $\varepsilon_2(\omega)$ requires the precise values of energy eigenvalues and electron wavefunctions. These are natural outputs of a band structure calculation.

In order to get the best optical spectra of the dielectric function $\varepsilon(\omega)$, a dense mesh of uniformly distributed *k*-points is required. Hence, the Brillouin zone (BZ) integration was performed with 657 points in the irreducible part of the Brillouin zone. Our calculated optical properties are scissor corrected [23] by 0.143 eV, this value is the difference between the calculated (2.927 eV) and measured (3.07 eV) [5] energy band gap. This could be traced to the fact that DFT calculations usually underestimate the energy gaps. For this reason we have used the scissor correction, which merely makes the calculated energy band gap equal to the experimental one. The dielectric function $\varepsilon(\omega)$ can be used to describe the linear response of the system to electromagnetic radiation, which is related to the interaction of photons with electrons.

Generally there are two contributions to $\varepsilon(\omega)$, namely due to intra-band and inter-band transitions. The contribution due to intra-band transitions is crucial only for metals. The inter-band transitions of the dielectric function $\varepsilon(\omega)$ can be split into direct and indirect transitions. We neglect the indirect inter-band transitions involving scattering of phonons assuming that they give a small contribution to $\varepsilon(\omega)$. To calculate the direct inter-band contributions to the imaginary part of the dielectric function $\varepsilon_2(\omega)$, it is necessary to perform summation over the BZ structure for all possible transitions from the occupied to the unoccupied states. Taking the appropriate transition matrix elements into account, we calculated the imaginary part of the dielectric functions $\varepsilon_2(\omega)$ using the expressions given in the Refs. [24,25].

Fig. 3 illustrates the imaginary and real parts of the electronic dielectric function $\varepsilon(\omega)$ spectrum for a radiation up to 20 eV. Our analysis $\varepsilon_2(\omega)$ curve shows that the threshold energy (first critical point) of the dielectric function occurs at 3.07 eV. This point is

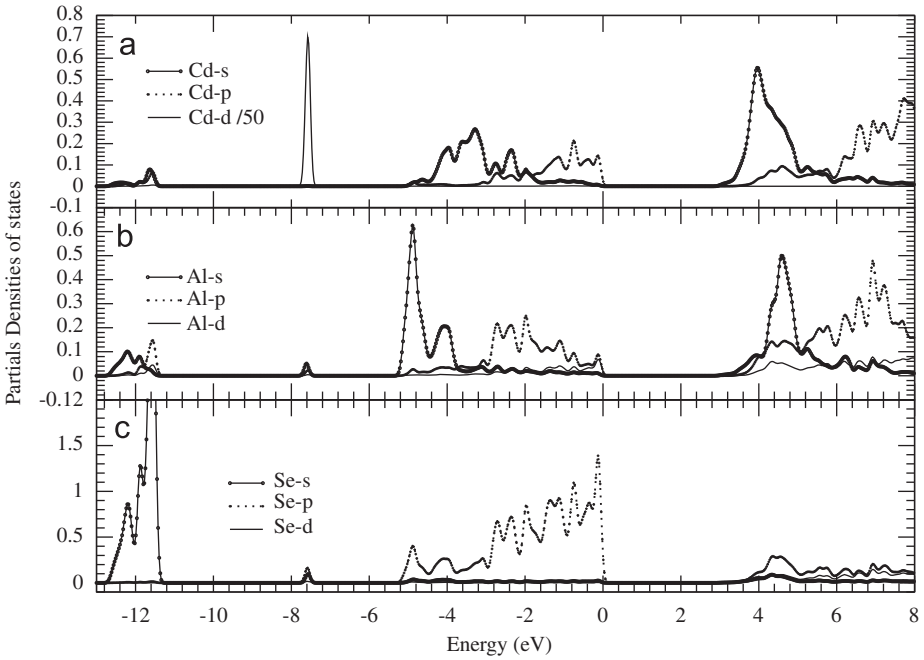

Fig. 2. Calculated partial densities of states for $CdAl_2Se_4$.

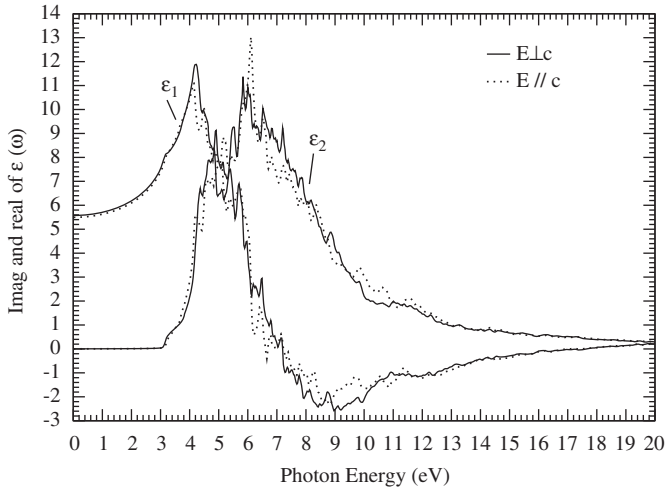

Fig. 3. Calculated imaginary and real parts of the frequency dependent dielectric function $\varepsilon(\omega)$ of $CdAl_2Se_4$: $\varepsilon_2^{\perp}(\omega)$ (*light solid curve*), $\varepsilon_2^{\parallel}(\omega)$ (light dotted curve), $\varepsilon_1^{\perp}(\omega)$ (*light solid curve*) and $\varepsilon_1^{\parallel}(\omega)$ (light dotted curve).

$\Gamma_v - \Gamma_c$ splitting which gives the threshold for direct optical transitions between the highest valence and the lowest conduction band. This is known as the fundamental absorption edge. The origin of these peaks is attributed to the inter-band transitions from the occupied Cd- (Al-) *p* and Se-*s* states to the unoccupied Cd- (Al-) *p* and Se-*d* states. Beyond these points, the curve increases rapidly. This is due to the fact that the number of points contributing towards $\varepsilon_2(\omega)$ increases abruptly. $\varepsilon_2^{\perp}(\omega)$ and $\varepsilon_2^{\parallel}(\omega)$ display one major peak situated at energies 5.8 and 6.2 eV, respectively. We note an insignificant hump on the left shoulder of the main peak situated at energies 4.8 and 5.2 eV for $\varepsilon_2^{\perp}(\omega)$ and $\varepsilon_2^{\parallel}(\omega)$, respectively. The magnitudes of $\varepsilon_2^{\perp}(\omega)$ and $\varepsilon_2^{\parallel}(\omega)$ maxima decrease when we move to higher energies. It is known that peaks in the optical response are caused by the electric–dipole transitions between the valence and conduction bands. In order to identify these peaks we need to consider the optical matrix

Table 2
Calculated, experimental and theoretical values of energy gap E_g(eV) and static constants $\varepsilon_1^{\perp}(0)$, $\varepsilon_1^{\parallel}(0)$, $n^{\perp}(0)$ and $n^{\parallel}(0)$.

	This work	Experimental	Theoretical
E_g(eV)	2.927	3.07[a] 3.082[b] (at 10 K)	2.13[c]
$\varepsilon_1^{\perp}(0)$	5.575	–	–
$\varepsilon_1^{\parallel}(0)$	5.496	–	–
$n^{\perp}(0)$	2.362	2.283[d] ± 0.005	–
$n^{\parallel}(0)$	2.344	2.264[d] ± 0.005	–

[a] Ref. [6].
[b] Ref. [11].
[c] Ref. [24].
[d] Ref. [4].

elements. At the low and high energy range both $\varepsilon_2^{\perp}(\omega)$ and $\varepsilon_2^{\parallel}(\omega)$ show isotropic behavior, while in the intermediate energies they show anisotropic behavior.

The real part $\varepsilon_1(\omega)$ of dielectric function can be evaluated from the imaginary part $\varepsilon_2(\omega)$ by using Kramer–Kronig relationship. The static dielectric constant $\varepsilon_1(0)$ is given by the low energy limit of $\varepsilon_1(\omega)$. Note that we do not include phonon contributions to the dielectric screening. $\varepsilon_1(0)$ corresponds to the static optical dielectric constant (ε_∞). The calculated value of $\varepsilon_1^{\perp}(0)$ and $\varepsilon_1^{\parallel}(0)$ are listed in Table 2. Our calculations show that there is a weak anisotropy between the extraordinary and ordinary components of $\varepsilon_1(\omega)$ and $\varepsilon_2(\omega)$.

The refractive index $n(\omega)$, the reflectivity $R(\omega)$ and electron energy loss function $L(\omega)$ can be derived from $\varepsilon_1(\omega)$ and $\varepsilon_2(\omega)$. In Fig. 4a and b, we show the calculated ordinary and extraordinary components of the refractive index $n(\omega)$ along with experimental data [4]. The refractive index spectrum shows a weak anisotropy between extraordinary and ordinary components. The refractive index reaches a maximum value of about 3.4 and 3.53 at 4.13 and 4.24 eV for $n^{\parallel}(\omega)$ and $n^{\perp}(\omega)$, respectively. The values of calculated $n^{\parallel}(0)$ and $n^{\perp}(0)$ are listed in Table 2. Generally a compound which shows considerable anisotropy in the linear optical susceptibilities

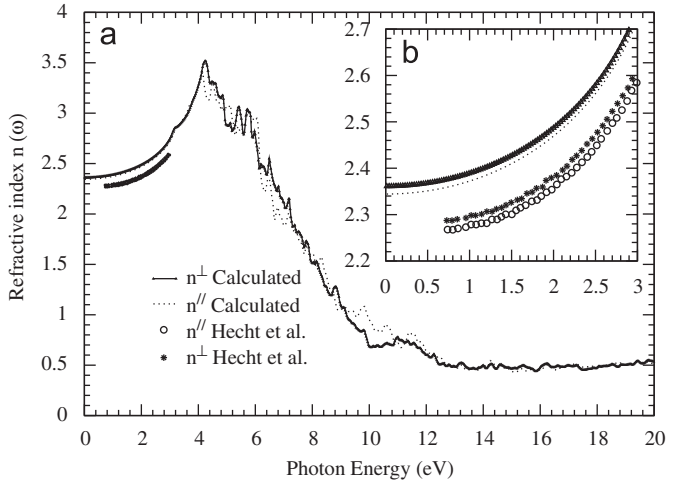

Fig. 4. Calculated refractive index $n(\omega)$ spectra of $CdAl_2Se_4$: $n^{\perp}(\omega)$ (*dark solid curve*), $n^{\parallel}(\omega)$ (light dotted curve) along with the experimental data [4]; (○-curve) $n^{\perp}(\omega)$ and (*-curve) $n^{\parallel}(\omega)$.

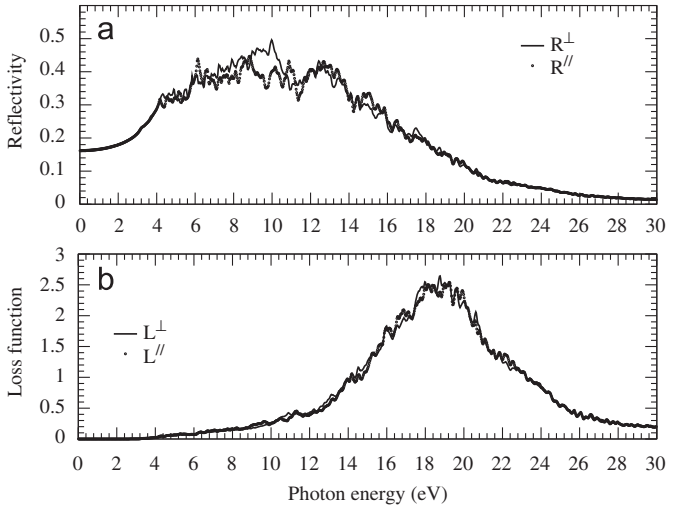

Fig. 5. (a) Calculated reflectivity spectra $R(\omega)$: $R^{\perp}(\omega)$ (*light solid curve*) and $R^{\parallel}(\omega)$ (light dotted curve). (b) Calculated loss function $L(\omega)$: $L^{\perp}(\omega)$ (*light solid curve*) and $L^{\parallel}(\omega)$ (light dotted curve).

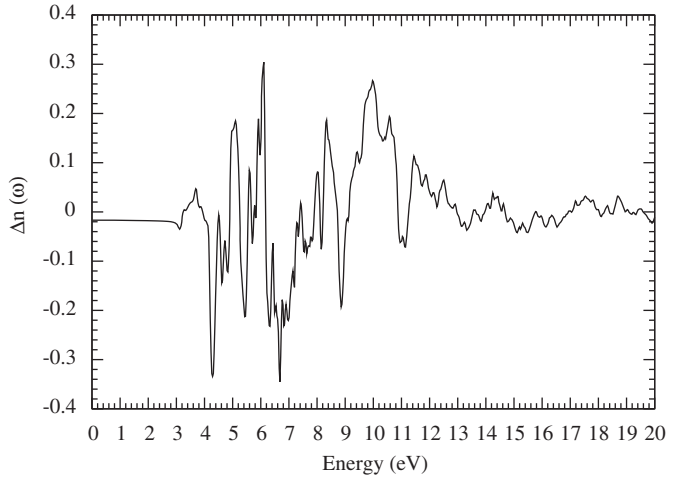

Fig. 6. Calculated $\Delta n(\omega)$ spectrum of $CdAl_2Se_4$ compound.

favors an important quantity in second harmonic generation (SHG) and optical parametric oscillator (OPO) due to better fulfilling of phase matching conditions, determined by birefringence. The birefringence is the difference between the extraordinary and ordinary refraction indices, $\Delta n = n_e - n_0$, where n_e is the index of refraction for an electric field oriented along the c-axis and n_0 is the index of refraction for an electric field perpendicular to the c-axis. Since this compound shows very weak anisotropy as a consequence it possesses small birefringence $\Delta n(\omega)$ (see Fig. 6). Birefringence is important only in the non-absorbing region, which is below the energy gap.

The reflectivity spectra for the ordinary and extraordinary components are shown in Fig. 5a. Again it shows a weak anisotropy between the two components. The energy loss function $L(\omega)$ (see Fig. 5b) shows the main peak in the energy loss function, which defines the screened plasma frequency ω_p [26], are located at 19.0 eV. This main peak corresponds to the abrupt reduction of the reflectivity spectrum $R(\omega)$ and to the zero crossing of $\varepsilon_1(\omega)$ (Fig. 6).

3.2.3. Second harmonic generation

The complex second-order nonlinear optical susceptibility tensor $\chi^{(2)}_{ijk}(-2\omega;\omega;\omega)$ can be generally written as the sum of three physically different contributions (see Ref. [27]). For simplicity we call $\chi^{(2)}_{ijk}(-2\omega;\omega;\omega)$ as$\chi^{(2)}_{ijk}(\omega)$. The subscripts i, j, and k are Cartesian indices. It is known from the previous work of Hahn et al. [28] that the structure of $CdAl_2Se_4$ is $I\overline{4}$. The lower symmetry of the defect chalcopyrites S_4 suggests that they will be uniaxial and may also have interesting nonlinear optical properties. While it is true that the lower symmetry will allow other nonzero components of the $\chi^{(2)}_{\{ijk\}} = 2d_{\{ijk\}}$ tensor, the magnitude of the $\chi^{(2)}$ is known to vary strongly with band gap and the latter is still poorly known. In the point group $\overline{4}2m = D_{2d}$, the symmetry allowed the components $d_{\{14\}} \equiv d_{\{xyz\}} = d_{\{25\}} \equiv d_{\{yxz\}}$ and $d_{\{36\}} \equiv d_{\{zxy\}}$ which are further more equal in the static limit by Kleinman symmetry. In the point group $\overline{4} = S_4$, the allowed components are all of the above and in addition: $d_{\{zxy\}}$, $d_{\{yxz\}}$, $d_{\{yzy\}}$, $d_{\{xxz\}}$, $d_{\{zyy\}}$ and $d_{\{zxx\}}$. Our calculated second-order nonlinear optical susceptibilities $\chi^{(2)}_{ijk}(\omega)$ are scissors corrected. $\chi^{(2)}_{ijk}(\omega)$ is very sensitive to the scissors correction. The scissors correction has a profound effect on magnitude and sign of $\chi^{(2)}_{ijk}(\omega)$. That is attributed to the fact that the DFT calculations underestimate the energy gaps. Hence when we use the scissors correction it will have a considerable effect on $\chi^{(2)}_{ijk}(\omega)$. It is well known that

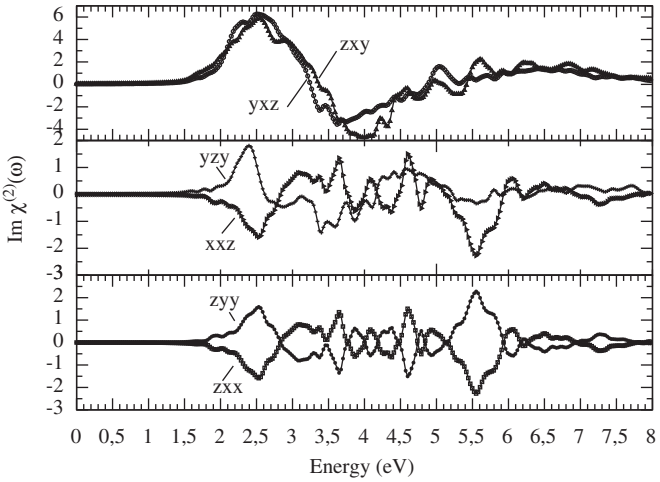

Fig. 7. Calculated $\mathrm{Im}\,\chi^{(2)}_{zxy}(\omega)$ and $\mathrm{Im}\,\chi^{(2)}_{yxz}(\omega)$ (upper panel), $\mathrm{Im}\,\chi^{(2)}_{yzy}(\omega)$ and $\mathrm{Im}\,\chi^{(2)}_{xxz}(\omega)$ (intermediate panel), $\mathrm{Im}\,\chi^{(2)}_{zyy}(\omega)$ and $\mathrm{Im}\,\chi^{(2)}_{zxx}(\omega)$ (lower panel). All $\mathrm{Im}\,\chi^{(2)}$ are multiplied by 10^{-7}, in esu units.

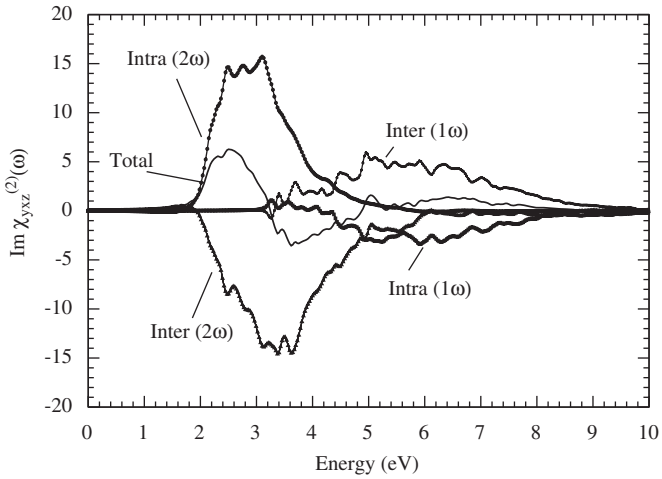

Fig. 8. Calculated total Im $\chi^{(2)}_{zxy}(\omega)$ spectrum along with the intra $(2\omega)/(1\omega)$- and inter $(2\omega)/(1\omega)$-band contributions. All Im $\chi^{(2)}$ are multiplied by 10^{-7}, in esu units.

nonlinear optical properties are more sensitive to small changes in the band structure than the linear optical properties. Hence any anisotropy in the linear optical properties is enhanced in the nonlinear spectra. This is attributed to the fact that the second harmonic response $\chi^{(2)}_{ijk}(\omega)$ involves 2ω resonance in addition to the usual ω resonance. Both the 2ω and ω resonances can be further separated into inter-band and intra-band contributions. The calculated imaginary part of the second harmonic generation (SHG) susceptibility is shown in Fig. 7. A definite enhancement in the anisotropy on going from linear optical properties to the nonlinear optical properties is evident (Fig. 7-first panel). We have calculated the total complex susceptibility of all nonzero components of $\chi^{(2)}_{ijk}(\omega)$. We established that $\chi^{(2)}_{zxy}(\omega)$ is the dominant component. We can identify the origin of the peaks in these figures as being $2\omega/\omega$ resonance of the peaks in the linear dielectric function. In Fig. 8, we show the ω and 2ω inter-/intra-band contributions to the Im $\chi^{(2)}_{zxy}(\omega)$ component. We note the opposite signs of the two contributions throughout the frequency range. As can be seen the total second harmonic generation susceptibility is zero below half the band gap. The 2ω terms start contributing at energies $\sim 1/2E_g$ and the ω terms for energy values above E_g. In the low energy regime (≤ 1.535 eV) the SHG optical spectra are dominated by the 2ω contributions. Beyond 3.07 eV (value of the fundamental energy gap) the major contribution comes from the ω term.

One would expect that the structures in Im $\chi^{(2)}_{ijk}(\omega)$ could be understood from the structures in $\varepsilon_2(\omega)$. Unlike the linear optical spectra, the features in the SHG susceptibility are very difficult to identify from the band structure because of the presence of 2ω and ω terms. But we can make use of the linear optical spectra to identify the different resonance leading to various features in the SHG spectra. The first structure in Im $\chi^{(2)}_{zxy}(\omega)$ and Im $\chi^{(2)}_{yxz}(\omega)$ between 1.535 and 3.5 eV is mainly from 2ω resonance and arises from the first structure in $\varepsilon_2(\omega)$. The second structure between 3.5 and 4.5 eV is associated with interference between a ω resonance and 2ω resonance and associated with high structure in $\varepsilon_2(\omega)$. The last structure from 4.5 to 5.5 is mainly due to ω resonance and associated with the tail in $\varepsilon_2(\omega)$.

4. Conclusion

The all electron full potential linearized augmented plane wave method has been used for an *ab initio* theoretical study of the band structure, total and partial density of states, and the spectral features of the linear and nonlinear optical susceptibilities. Our calculations show that the valence band maximum (VBM) and the conduction band minimum (CBM) are located at the Γ point resulting in a direct band gap of about 2.927 eV. Our calculated energy band gap is very close to the experimental one (3.07 eV). This agreement is attributed to the fact that the Engel–Vosko GGA formalism optimizes the corresponding potential for the band structure calculations. The ground state quantities such as lattice parameters (a, c, x, y and z), bulk modules B and its pressure derivative B' are evaluated. We found that they are in reasonable agreement with the available experimental data and theoretical calculations. To complete the fundamental characteristics of the investigated compound, we have calculated and analyzed their linear and nonlinear optical susceptibilities. We have calculated the total complex susceptibility of all nonzero components of $\chi^{(2)}_{ijk}(\omega)$ and we found that $\chi^{(2)}_{zxy}(\omega)$ is the dominant component. We demonstrate the effect of using a full potential on the band structure, density of states, and the linear and nonlinear optical susceptibilities.

Acknowledgments

We would like to thank the Theoretical Physics Laboratory (LPT) Tlemcen, for the support equipment and finance. For the author Ali Hussain Reshak, the work was supported from the institutional research concept of the Institute of Physical Biology, UFB (no. MSM6007665808).

References

[1] J.L. Shay, J.H. Wernik, Ternary chalcopyrite semiconductors: growth, electronic properties and applications, Pergamon Press, Oxford, 1974.
[2] M.A. Gabor, J.R. Tuttle, D.S. Albin, M.A. Contreras, R. Nou, A.M. Hermann, Appl. Phys. Lett. 65 (1994) 198.
[3] M. Fuentes-Cabrera, O.F. Sankey, J. Phys. Condens. Matter 13 (2001) 1669.
[4] J.-D. Hecht, A. Eifler, V. Riede, M. Schubert, G. Krauß, V. Krämer, Phys. Rev. B 57 (1998) 7037.
[5] G. Krauß, V. Krämer, A. Eifler, V. Reide, S. Wenger, Cryst. Res. Technol. 32 (1997) 223.
[6] A.N. Georgobiani, S.I. Radautsan, I.M. Tiginyanu, Sov. Phys. Semicond. 19 (1985) 121.
[7] S.I. Radautsan, I.M. Tiginyanu, Jpn. J. Appl. Phys. 32 (Suppl. 3) (1993) 5.
[8] L. Garbato, F. Ledda, R. Rucci, Prog. Cryst. Growth Charact. 15 (1987) 1–41.
[9] S. Meenakshi, V. Vijyakumar, B.K. Godwal, A. Eifler, I. Orgzall, S. Tkachev, H.D. Hochheimer, J. Phys. Chem. Solids 67 (2006) 1660.
[10] K.J. Range, W. Becker, A. Weiss, Z. Naturf. B 23 (1968) 1261.
[11] X. Jiang, W.R.L. Lambrecht, Phys. Rev. B 69 (2004) 035201.
[12] A. Eifler, J.-D. Hecht, G. Lippold, V. Reide, W. Grill, G. Krauß, V. Krämer, Physica B 263–264 (1999) 806.
[13] G.K.H. Madsen, P. Blaha, K. Schwarz, E. Sjöstedt, L. Nordström, Phys. Rev. B 64 (2001) 195134.
[14] K. Schwarz, P. Blaha, G.K.H. Madsen, Comput. Phys. Commun. 147 (2002) 71.
[15] P. Blaha, K. Schwarz, G.K.H. Madsen, D. Kvasnicka, J. Luitz, WIEN2k, an augmented plane wave plus local orbitals program for calculating crystal properties, Vienna University of Technology, Vienna, Austria, 2001.
[16] Z. Wu, R.E. Cohen, Phys. Rev. B 73 (2006) 235116.
[17] A. Shaukat, Y. Saeed, N. Ikram, H. Akbarzadeh, Eur. Phys. J. B 62 (2008) 439.
[18] F.D. Murnaghan, Proc. Nat. Acad. Sci. USA 30 (1947) 244;
J.R. Macdonald, D.R. Powell, J. Res. Nat. Bur. Stand. A 75 (1971) 441.
[19] P. Dufek, P. Blaha, K. Schwarz, Phys. Rev. B 50 (1994) 7279.
[20] E. Engel, S.H. Vosko, Phys. Rev. B 47 (1993) 13164.
[21] L. Lykke, B. Iversen, G.K.H. Madsen, Phys. Rev. B 73 (2006) 195121.
[22] S.M. Baizaee, N. Mousavi, Phys. B Condens. Matter 404 (2009) 2111.
[23] J.L.P. Hughes, J.E. Sipe, Phys. Rev. B 53 (1996) 10751.
[24] S. Hufner, R. Claessen, F. Reinert, Th. Straub, V.N. Strocov, P. Steiner, J. Electron Spectrosc. Relat. Phenom. 100 (1999) 191;
R. Ahuja, S. Auluck, B. Johansson, M.A. Khan, Phys. Rev. B 50 (1994) 2128.
[25] A. Hussain Reshak, I.V. Kityk, S. Auluck, J. Chem. Phys. 129 (2008) 074706.
[26] M. Fox, Optical Properties of Solids, Academic Press, New York, 1972.
[27] A.H. Reshak, Ph.D. Thesis, Indian Institute of Technology, Rookee, India, 2005.
[28] H. Hahn, G. Franck, W. Kligler, A.D. Störger, Z. Anorg. Allg. Chem. 279 (1955) 241.